Radial Collapse of Single-Walled Carbon Nanotubes Induced by the Cu_2O Surface

KeYou Yan, QingZhong Xue,* QingBin Zheng, Dan Xia, Huijuan Chen, and Jie Xie

College of Physics Science and Technology, China University of Petroleum, Dongying, Shandong 257061, P. R. China

Received: September 17, 2008; Revised Manuscript Received: November 5, 2008

We studied the radial collapse of single-walled carbon nanotubes (CNTs) on the Cu_2O surface using molecular dynamic simulations. When the diameter of CNTs exceeds a threshold, the CNTs approach the Cu_2O surface and collapse spontaneously by the van der Waals force between the CNTs and the Cu_2O surface. Because the collapsed CNTs are much more like graphenes, this collapse process of CNTs seems the reverse process of folding graphene nanoribbons to form CNTs. The collapsed CNTs exhibit as linked graphene ribbons and have the largest area to contact with the Cu_2O surface, which greatly enhances adhesion between the CNTs and the Cu_2O surface and keeps the system much more stable. Due to the hydrophobic properties of CNTs, the collapsed CNTs on the oxide surface can isolate the metal oxide from water solution, which suggests that the collapsed CNTs on the metal oxide surfaces have potential applications in corrosion protection and scale inhibition fields.

1. Introduction

Carbon nanotubes (CNTs), due to their unique structure and properties, hold great promise as excellent materials for potential applications in composites and nanosized electronical and mechanical devices.[1−5] However, the CNTs' excellent properties can be affected by the CNTs' deformation and collapse, which have been observed in experimental and theoretical works.[4,6−19] Lourie et al. reported an axial deformation mode resulting from the embedment of the tubes in a polymer matrix, where the CNTs were transformed into bends and loops, and it's the first estimation of the strength of CNTs under compressive stresses.[4] Some other researchers also observed such CNTs deformation under other external forces, such as electron beam pressure[11] and hydrostatic pressure.[8,12,16−18] Besides, Chopra et al. discovered several ribbon structures of collapsed CNTs, which were synthesized on the surface of copper cathode by a carbon-arc discharge method. They suggested that the collapsed CNTs formed when a conventional hollow cylindrical nanotube was locally deformed (for example, kinked or twisted) by external mechanical forces.[6] The deformation and collapse of CNTs are sometimes considered to confine their practical applications because the pristine structures have been destroyed. Therefore, it is vital to study the defective mechanics of CNTs and exploit the advantage of the collapsed CNTs, which can make us understand this nanostructure clearly and enable numerous new applications.

Recently, Yu et al. demonstrated a new method of synthesizing CNTs using first principles and classical molecular dynamics simulations (MD). They found that the CNTs can be formed by folding graphene nanoribbons patterned on graphite films through adsorption of atoms of varying coverage, which introduced an external stress to drive the folding process.[20] Thus, there seems to be some relationship between the graphene nanoribbons and the CNTs.

In this paper, we study the radial deformation and collapse of single-walled CNTs on the Cu_2O surface using MD simulations. It is demonstrated that when the diameter of CNTs exceeds a threshold, the CNTs approach the Cu_2O surface and then collapse spontaneously by the van der Waals force between the CNTs and the Cu_2O surface. Because the collapsed CNTs are much more like graphenes, the collapse process of the CNTs seems to be the reverse process of folding graphene nanoribbons to form CNTs spontaneously. The results demonstrate that the Cu_2O surface may play an important role in formation of the collapsed CNTs in the experimental work above.[6] Owing to the different properties of the CNTs and Cu_2O surface and the strong interaction between them the heterojunctions formed by the CNTs and Cu_2O may gain considerable interest in nanosized electronical applications.[21−26]

2. Simulation Methods

2.1. Force Field. Molecular mechanics (MM) and MD simulations have been carried out using a commercial software package called MATERIALS STUDIO developed by Accelrys Inc. The condensed phase optimization molecular potentials for atomistic simulation studies (COMPASS) module in the MATERIALS STUDIO software is used to conduct force-field computations. The COMPASS is a parametrized, tested, and validated first ab initio force field,[27,28] which enables an accurate prediction of various gas-phase and condensed-phase properties of most of the common organic and inorganic materials.[29−31]

Application of quantum mechanical techniques can accurately simulate a system of interacting particles, but such techniques often cost too much time and are usually feasible only in systems containing up to few hundreds of interacting particles. To our knowledge, the main goal of simulations of the systems containing a large number of particles is generally to obtain the systems' bulk properties which are primarily controlled by the location of atomic nuclei. However, knowledge of the electronic structure, provided by the quantum mechanic techniques, is not critical. Thus, we could have good insight into the behavior of a system if a reasonable, physically based approximation of the potential (force field) can be obtained, which can be used to generate a set of system configurations which are statistically consistent with a fully quantum mechan-

* To whom correspondence should be addressed. E-mail: xueqingzhong@tsinghua.org.cn.

10.1021/jp808264d CCC: $40.75 © 2009 American Chemical Society
Published on Web 01/30/2009

ical description. As stated above, a crucial point in the atomistic simulations of multiparticle systems is the choice of the force fields, a brief overview of which is given in this section.

In general, the total potential energy of a molecular system includes the following terms

$$E_{\text{total}} = E_{\text{valence}} + E_{\text{cross-term}} + E_{\text{nonbond}} \quad (1)$$

$$E_{\text{valence}} = E_{\text{bond}} + E_{\text{angle}} + E_{\text{torsion}} + E_{\text{oop}} + E_{\text{UB}} \quad (2)$$

$$E_{\text{cross-term}} = E_{\text{bond-bond}} + E_{\text{angle-angle}} + E_{\text{bond-angle}} + E_{\text{end-bond-torsion}} + E_{\text{middle-bond-torsion}} + E_{\text{angle-torsion}} + E_{\text{angle-angle-torsion}} \quad (3)$$

$$E_{\text{nonbond}} = E_{\text{vdW}} + E_{\text{Coulomb}} + E_{\text{H-bond}} \quad (4)$$

The valence energy, E_{valence}, generally includes a bond stretching term, E_{bond}, a two-bond angle term, E_{angle}, a dihedral bond−torsion term, E_{torsion}, an inversion (or out-of-plane interaction) term, E_{oop}, and a Urey−Bradlay term (involves interactions between two atoms bonded to a common atom), E_{UB}. The cross-term interacting energy, $E_{\text{cross-term}}$, generally includes stretch−stretch interactions between two adjacent bonds, $E_{\text{bond-bond}}$, bend−bend interactions between two valence angles associated with a common vertex atom, $E_{\text{angle-angle}}$, stretch−bend interactions between a two-bond angle and one of its bonds, $E_{\text{bond-angle}}$, stretch−torsion interactions between a dihedral angle and one of its end bonds, $E_{\text{end-bond-torsion}}$, stretch−torsion interactions between a dihedral angle and its middle bond, $E_{\text{middle-bond-torsion}}$, bend−torsion interactions between a dihedral angle and one of its valence angles, $E_{\text{angle-torsion}}$, and bend−bend−torsion interactions between a dihedral angle and its two valence angles, $E_{\text{angle-angle-torsion}}$. The nonbond interaction term, E_{nonbond}, accounts for the interactions between nonbonded atoms and includes the van der Waals energy, E_{vdW}, the Coulomb electrostatic energy, E_{Coulomb}, and the hydrogen-bond energy, $E_{\text{H-bond}}$.

In COMPASS the parametrization procedure can be divided into two phases: ab initio parametrization and empirical optimization. In the first phase, partial charges and valence parameters are derived by fitting to ab initio potential-energy surfaces. At this point, the van der Waals parameters are fixed to a set of initial approximated parameters. In the second phase, emphasis is on optimizing the force field to yield good agreement with experimental data. A few critical valence parameters are adjusted based on the gas-phase experimental data. More importantly, the van der Waals parameters are optimized to fit the condensed-phase properties. For covalent molecular systems, this refinement is done based on MD simulations of liquids; for inorganic systems, this is based on energy minimization on crystals. The COMPASS force field uses different expressions for various components of the potential energy as follows[29,30]

$$E_{\text{valence}} = \sum_b [K_2(b-b_0)^2 + K_3(b-b_0)^3 + K_4(b-b_0)^4] + \sum_\theta [H_2(\theta-\theta_0)^2 + H_3(\theta-\theta_0)^3 + H_4(\theta-\theta_0)^4] + \sum_\varphi [V_1[1-\cos(\varphi-\varphi_1^0)] + V_2[1-\cos(2\varphi-\varphi_2^0)] + V_3[1-\cos(3\varphi-\varphi_3^0)]] + \sum_x K_x\chi^2 + E_{\text{UB}} \quad (5)$$

$$E_{\text{cross-term}} = \sum_b \sum_{b'} F_{bb'}(b-b_0)(b'-b_0') + \sum_\theta \sum_{\theta'} F_{\theta\theta'}(\theta-\theta_0)(\theta'-\theta_0') + \sum_b \sum_\theta F_{b\theta}(b-b_0)(\theta-\theta_0) + \sum_b \sum_\theta F_{b\theta}(b-b_0)[V_1\cos\varphi + V_2\cos 2\varphi + V_3\cos 3\varphi] + \sum_{b'} \sum_\theta F_{b'\theta}(b'-b_0')(b'-b_0')[F_1\cos\varphi + F_2\cos 2\varphi + F_3\cos 3\varphi] + \sum_\theta \sum_\varphi F_{\theta\varphi}(\theta-\theta_0)[V_1\cos\varphi + V_2\cos 2\varphi + V_3\cos 3\varphi] + \sum_\varphi \sum_\theta \sum_{\theta'} K_{\varphi\theta\theta'}\cos\varphi(\theta-\theta_0)(\theta'-\theta_0') \quad (6)$$

$$E_{\text{nonbond}} = \sum_{i>j}\left[\frac{A_{ij}}{r_{ij}^9} - \frac{B_{ij}}{r_{ij}^6}\right] + \sum_{i>j}\frac{q_iq_j}{\varepsilon r_{ij}} + E_{\text{H-bond}} \quad (7)$$

where q is the atomic charge, ε is the dielectric constant, and r_{ij} is the $i-j$ atomic separation distance. b and b' are the lengths of two adjacent bonds, θ is the two-bond angle, ϕ is the dihedral torsion angle, and χ is the out of plane angle. b_0, $k_i(i = 2-4)$, θ_0, $H_i(i = 2-4)$, $\phi_i^0(i = 1-3)$, $V_i(i = 1-3)$, $F_{bb'}$, b_0', $F_{\theta\theta'}$, θ_0', $F_{b\theta}$, $F_{b\phi}$, $F_{b'\theta}$, $F_i(i = 1-3)$, $F_{\theta\phi}$, $K_{\phi\theta\theta'}$, A_{ij}, and B_{ij} are fitted from quantum mechanics calculations and are implemented into the Discover module of Materials Studio, a powerful commercial atomic simulation program used in this paper.

2.2. Simulation Details. The designed system consisted of O-terminated Cu_2O (001) lattice plane of 17.078 Å thickness, which was constructed as a supercell in the range of 42.696 × 42.696 × 56.011 Å^3 and CNTs with a length of 24.6 Å and different diameters and chiralities. The unsaturated boundary effect of CNT was avoided by adding hydrogen atoms. Each C−C bond length was 1.42 Å, and the C−H bond length was 1.14 Å. The surface and CNTs were optimized by the smart minimizer method to obtain the surface effect structure and reasonable cylinder geometrics, respectively. In the CNTs, hydrogen atoms had charges of +0.1268 e and the carbon atoms connecting hydrogen atoms had charges of +0.1268 e; thus, the neutrally charged SWNTs were constructed. On the surface the copper atoms had charges of +0.4 e and the oxygen atoms had charges of 0 e. The charges and potential energy of the atoms were parametrized by the assigned COMPASS force field automatically when you performed the simulations. As initial configurations a series of CNTs was aligned parallel to the fixed Cu_2O (001) plane which were separated by 7 Å plus the radius size of the CNT and the Cu_2O (001) plane was parallel to the $x-y$ plane. Besides, in order to investigate the effect of different orientations and separations some other placements of the CNTs were also studied. The cutoff distance was 9.5 Å, and the permittivity of free space in the complex was six, which was similar to the electronic double layer in solution. The models were put into an NVT ensemble simulation at 300 K. Then the full-precision trajectory was recorded, and the results were analyzed.

3. Results and Discussion

Approach and Collapse Process. The snapshots of the CNT (10, 10) spontaneously approaching to the Cu_2O surface, shown in Figure 1, exhibit that the approach and collapse of the CNT (10, 10) happened subsequently. First, the CNT (10, 10) stretches its cross section from a circle to an oval along the normal direction of the Cu_2O surface and tries to touch it. When the bottom of the CNT(10, 10) reaches the Cu_2O surface the center of mass along the z direction (z-COM) of the CNT (10, 10)

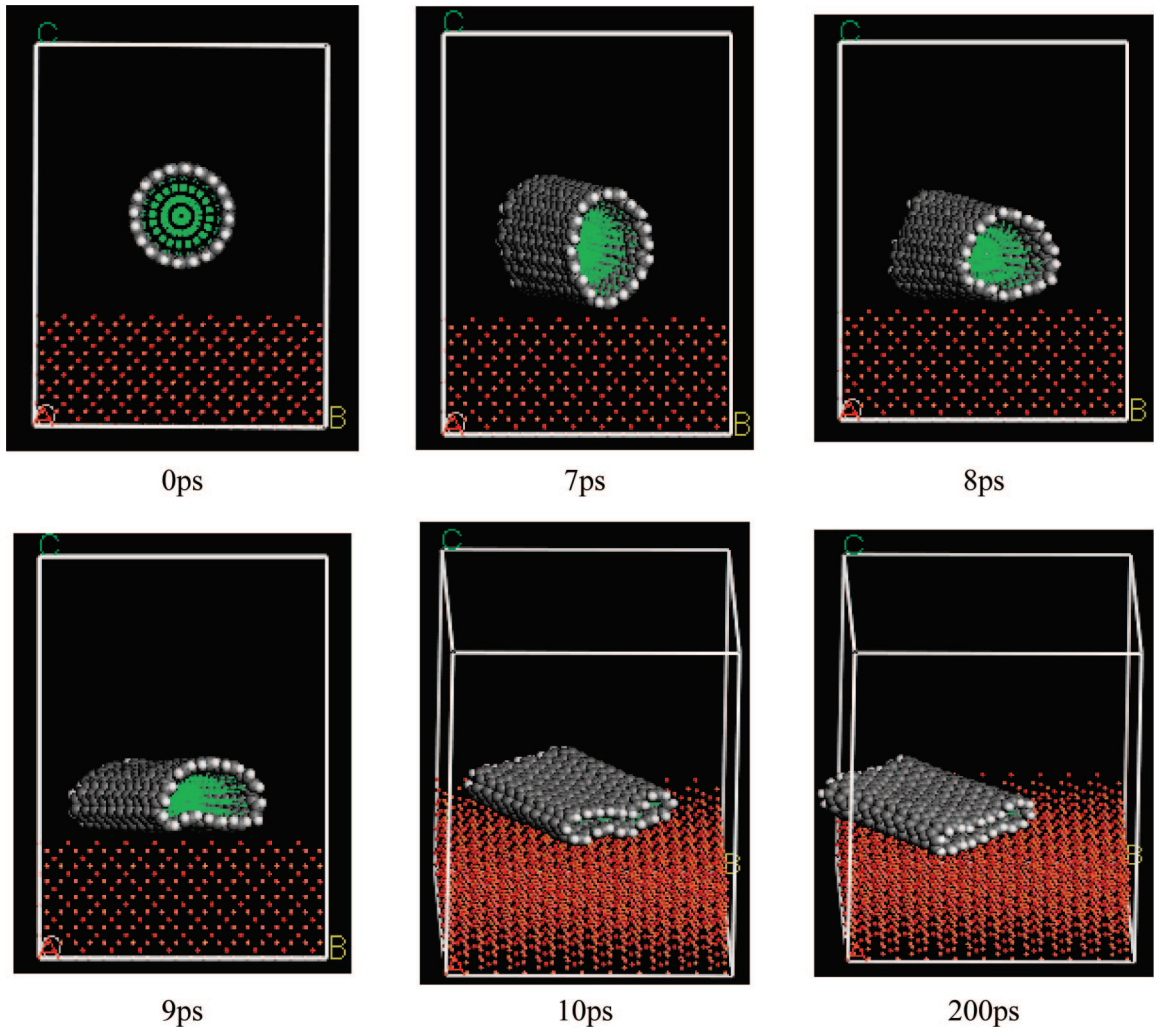

Figure 1. Simulation snapshots of the approach and collapse of the CNT (10, 10) on the Cu_2O surface at 0, 7, 8, 9, 10 and 200 ps.

varies from 30.858 to 26.903 Å and the shape of the CNT (10, 10) changes from cylindrical to oval along the parallel direction to the surface at $t = 7$ ps. At $t = 8$ ps the bottom layer of the collapsed CNT (10, 10) has adhered to the Cu_2O surface partially and the cross section of the CNT (10, 10) is transformed into a delta shape. After $t = 10$ ps the CNT(10, 10) spreads as a linked double graphitic layer paralleling the Cu_2O surface and fully collapses to cover the Cu_2O surface like a ribbon with a thickness of about 4 Å. The final z-COM is 20.75 Å, which is about 3.7 Å away from the Cu_2O surface. Such a short-haul distance indicates that the adhesion energy between the collapsed CNT and the Cu_2O surface is very strong. After these relaxations the total system energy approximately remains constant and the system reached equilibrium. From the whole process it can be concluded that the carbon atoms in the bottom semicircular tube require less time to reach equilibrium, whereas the top semicircular tube moves slowly to the surface and needs more time to reach equilibrium. This is consistent with the fact that the interaction between the bottom semicircular tube and the Cu_2O surface is stronger than that between the top semicircular tube and the Cu_2O surface. The equilibrium between the collapsed CNT and the Cu_2O surface is obviously a result of the balance between the repulsive and attractive van de Waals forces experienced by all atoms involved in such an interfacial region.

Geometric Deformation. In order to characterize the geometric deformation of the collapse CNT clearly the concentration profiles of the initial CNT (10, 10) and the collapsed CNT (10, 10) are shown in Figure 2. By the way, here we manually placed the initial CNT (10, 10) and the collapsed CNT (10, 10) in a box with the same COM and orientation for comparison. There is little difference in the concentration profile along the x axis between the initial CNT and the collapsed CNT, which illuminates that there is no deformation along the CNT's axial direction. However, the concentration profile along the y axis of the collapsed CNT becomes broad and flat and the concentration profile along the z axis of the collapsed CNT changes from the wide-serration shape to the shape with two narrow peaks. As shown in Table 1, some peak coordinates have been picked out from the concentration profiles to reflect the geometric deformation, and Δ denotes the difference between the peak coordinates along the (x, y, z) axis. Obviously, Δy and Δz of the initial CNT are approximately equal, which refers to the circular CNT (10, 10) with 13.56 Å diameter, and $\Delta x = 24.98$ Å denotes the equal length of the initial CNT (10, 10) and the collapsed CNT (10, 10) because of no deformation along the x axis between them. It is clearly seen from the concentration profile details that the collapsed CNT (10, 10) covered on the Cu_2O surface just like a $24.98 \times 18.58 \times 3.9$ Å^3 ribbon and the deformation energy of the ribbon is 449.63 kcal/mol. This collapsed CNT seems to exist stably because when we perform a geometric optimization, their configurations have little deformation. Due to the $\pi-\pi$ stacking of the linked collapsed CNT layers the collapsed CNT will cost even larger energy to transform back into its pristine structure. Thus, the geometric

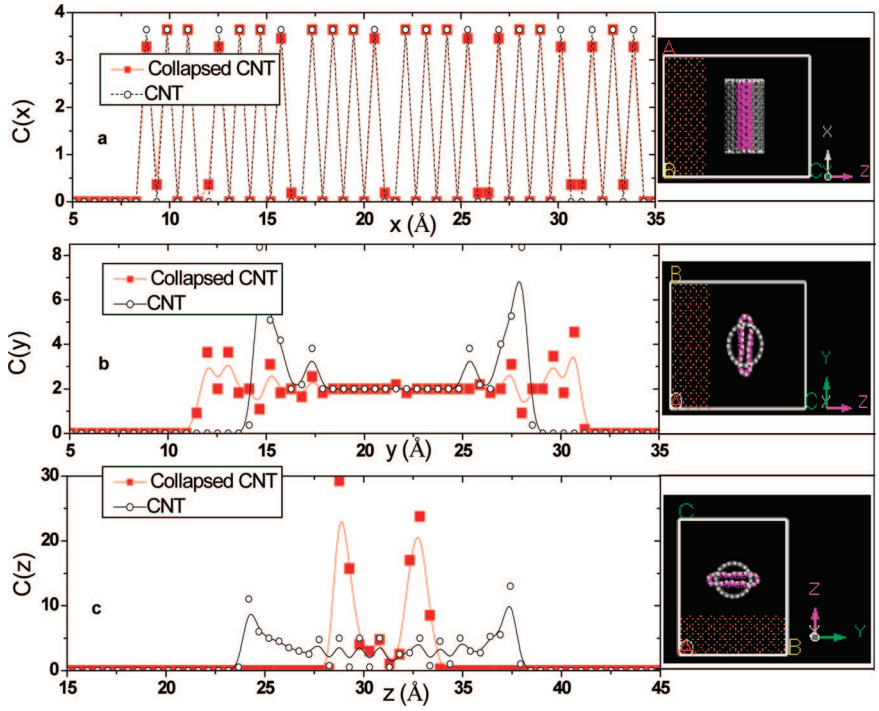

Figure 2. Concentration profiles of the CNT (10, 10) and collapsed CNT (10, 10) along the *x*, *y*, and *z* axes. The inset is the scheme of the placement in the box. The CNT and collapsed CNT are placed along *x* axis and parallel to the *x*−*y* surface with the same COM position.

TABLE 1: Peak Details in Concentration Profiles of CNT (10, 10) and Collapsed CNT (10, 10)

	initial CNT			collapsed CNT		
axis	first peak (Å)	last peak (Å)	Δ (Å)	first peak (Å)	last peak (Å)	Δ (Å)
x	8.76	33.74	24.98	8.76	33.74	24.98
y	14.49	28.07	13.58	12.09	30.68	18.58
z	24.18	37.46	13.38	28.7	32.6	3.9

conformation of the collapsed CNTs is another relatively stable or metastable structure in nature, which is consistent with Liu's argument that the collapsed CNTs are one of the three different energetically favorable structures.[10,19]

Interface Characteristics. The information of the interfacial region of the final structure can be characterized by the concentration profile of the combination, consisting of the CNT (10, 10) and the outmost surface layer Cu_2O, as shown in Figure 3. In Figure 3, d, d_1 and d_2 denote the distances between two peaks. d_1 expresses the distance between the inner layer of the collapsed CNT and the Cu_2O surface, and $d_2 = 3.9$ Å expresses the distance between the double linked layers of the collapsed CNT. As marked in Figure 3, d_1 was 2.68 Å, less than the shortest distance of the graphite layer 3.4 Å, which has almost entered the strong adhesive binding region of the chemical bond. The interaction between the collapsed CNT and the Cu_2O surface is strong because the collapsed CNT's π electrons and the O-terminated Cu_2O's dangling electrons stack when $d_1 =$ 2.68 Å. In order to discuss the contact intensity further, the interaction energy and specific binding energy are introduced to reflect the adhesion between the CNT and the Cu_2O surface. The interaction energy is defined as follows[32]

$$E_{\text{interaction}} = E_{\text{total}} - (E_{\text{CNT}} + E_{\text{surface}}) \quad (8)$$

where E_{total} is the energy of the system including CNT and the Cu_2O surface, E_{CNT} is the energy of CNT without the surface, and E_{surface} is the energy of Cu_2O surface without CNT, respectively. The specific binding energy is the interaction energy per unit contact area. The interaction energy and the specific binding energy between the CNT (10, 10) and the Cu_2O surface reached −294.12 kcal/mol and −0.634 kcal/ mol·Å^2, respectively. In other words, the adhesion between them is so strong that it is difficult to remove the CNT from the Cu_2O surface again.

Because these collapsed CNT ribbons afford larger area to cover the Cu_2O surface and the interface adhesion is very strong, the collapsed CNTs can isolate the metal oxide from water solution to inhibit chemical reaction between them due to the CNTs' hydrophobic properties. Therefore, the CNTs adhered to metal oxide surface have potential applications in corrosion protection and scale inhibition fields.

Physical Mechanism. To reveal the physical mechanisms of the approach and collapse of CNTs we tracked some kinds of energies in the system as shown in Table 2, where the total energy consists of the internal energy and the nonbond energy and the nonbond energy consists of the van der Waals energy and the electrostatic energy. The decrease of total energy of the system indicates that this approach and collapse behavior is a process of energy reduction, which is in accordance with the lowest energy theory. When the total energy reaches the minimum energy state the full collapse of CNT happens. From the energy differences between the initial structure and the final structure we find that the van der Waals energy has decreased a lot and finally reaches the minimum energy state, where the repulsive and attractive van der Waals forces reach equilibrium eventually. It is clear that the van der Waals force is the main drive for the CNTs to approach the Cu_2O surface. Thus, we reach a conclusion that the van der Waals interaction plays an

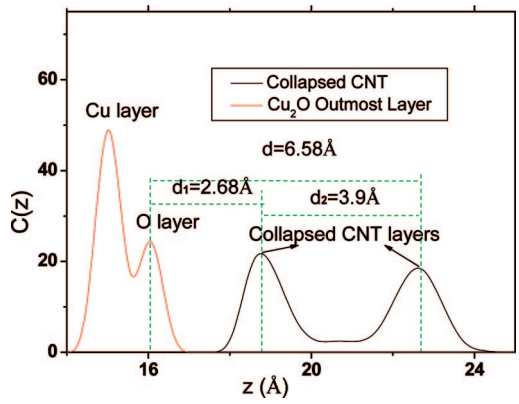

Figure 3. Concentration profile of the combination formed by the CNT (10, 10) and the outmost surface layer Cu_2O.

TABLE 2: Energy Details of Initial and Final Structures in the Simulation System

energy (kcal/mol)	initial structure (E_1)	final structure (E_2)	$\Delta E = E_2 - E_1$
total energy	18587.224947	18439.004528	−148.22042
internal energy	18440.035914	18633.314737	193.27882
nonbond energy	475.524032	134.024790	−341.49924
van der Waals energy	464.734297	148.029961	−316.70434
electrostatic energy	10.789735	−14.005170	−24.79491

important role in the approach and collapse process. During this process the van der Waals energy has partially transformed to the internal energy for geometry deformation of CNT and made the whole system energy decease. As a result, the collapsed CNTs have the largest area to contact with the Cu_2O surface, which greatly enhances the adhesion between the CNTs and the Cu_2O surface and keeps the system much more stable.

Influence Factors Analysis. The CNTs' approach and collapse on the Cu_2O surface depends on their diameter sizes. CNTs with different diameters have been selected for this observation, as shown in Figure 4. We find that when the CNT diameter is larger than a threshold the total energy of the CNT−Cu_2O system decreases quickly with increasing simulation time first when the CNT approaches to the surface and then reaches a relatively stable value with little fluctuations, which demonstrates that the CNT has fully collapsed. However, when the CNT diameter is smaller than the threshold the total energy of the CNT−Cu_2O system fluctuates with the simulation time for a while; after that the total energy decreases quickly with increasing simulation time when the CNT approaches the surface and then reaches a metastable state with larger fluctuations, which demonstrates that the CNTs are a little deformed but not fully collapsed. It is concluded that the approach can reduce the total energy of the system and make the total energy of the system reach a stable and lower state.

The interaction energies of the transitional structures (when CNTs just reach the surface) and final structures and the deformation energies of the CNTs with different diameters are shown in Figure 5. We find that when the CNT diameter reaches 8.14 Å the CNTs' semicollapse happens and the corresponding interaction energy increases a lot, and when the CNT diameter reaches 10.85 Å the CNTs' full collapse happens and the corresponding interaction energy increases more largely than that of the semicollapsed CNTs−Cu_2O surface. Therefore, the diameter threshold of armchair CNTs, where the full collapse happens, is about 10 Å. The fully collapsed CNTs have the largest area to contact with the Cu_2O surface and the largest interaction energy between the CNT and the Cu_2O surface, which can greatly enhance the adhesion between the CNT and the Cu_2O surface and keep the system much more stable.

In Figure 5b the different increasing trends of the final deformation energies of the CNTs exhibit the threshold where the CNT collapse happens, as shown by watershed of the two different fit lines. The fit lines exhibit different linear relationships of deformation energy versus diameter size, which can be expressed by the formulas in the scheme. Here, the semicollapse of CNTs cannot be reflected as the interaction energy versus diameter size because dynamic simulation also brings isotropic deformation, which enshrouds the increase of the deformation energy induced by semicollapsed to some extent.

In order to explain the deformation mechanics of the tubes, we introduce the specific energy for different compression ratios of round tubes; the relationship of specific energy correlated with the D/t ratio and compression ratio δ/D can be written as[33,34]

$$\text{specific energy} = c_1 e^{c_2 \delta/D} (D/t)^{-c_3} \; (c_1, c_2, c_3 = \text{constant}, c_1, c_2, c_3 > 0) \quad (9)$$

where D is the diameter of the CNT, t (3.4 Å) is the thickness of the wall, and δ is the compression strain of the CNT. It is clear that the energy absorbing capacity of tubes exponentially decreases rapidly with the increase of D/t ratio at first and infinitely approaches zero after a threshold. In other words, only a little energy can induce the variation of the compression ratio when the diameter of the CNT is larger than the threshold. Thus, the CNTs with larger diameters collapse easily and a critical diameter value exists when the CNTs suffer a given external force. Briefly, if the CNT is too slender, the benzene plane will be bent too much when lateral collapse happens, which needs plenty of energy. Therefore, the collapsed CNTs with a larger diameter are more stable; this is attributed to the fact that a larger area contact and a relatively stronger van der Waals interaction exists between the collapsed CNT with a larger diameter and the Cu_2O surface, which is consistent with the results that d_1, d_2, and d of the collapsed CNTs decrease a little with increasing diameters. This size effect is similar with the diameter dependence of critical deformation pressure when the hydrostatic pressures are applied on CNTs, where the critical deformation pressure decreases with increasing diameter.[7,16]

In addition, the size effect of the CNTs' lengths is considered. We vary the CNTs' length by setting the number of repeat units of the armchair CNTs as 5, 10, and 15 and then perform the same simulations. We find that the initial deformation usually begins at one side and then the further deformation passes from this side to the other along the longitudinal direction like dominoes in 10 repeat units CNT and 15 repeat units CNT. It is indicated that the domino effect also exists in this deformation as recent work demonstrates.[35] When the CNT length gets larger, the domino effect gets more visible. However, the length effect does not determine whether the collapse happens or not.

The chirality dependences of the interaction energy, d_1, d_2, and d, and the deformation energy have also been studied, as shown in Figure 6. The CNTs with different chiralities and similar sizes were performed in the simulations, and we find that the CNT chirality has little effect on the CNT collapse, although the double layers of the collapsed CNTs have geometrically conformed diversely by chirality as different rolled graphite shells, which is consistent with previous results in other systems by the atomic scale finite-element method.[10,18] The chirality dependence indicates that the structural and mechanical

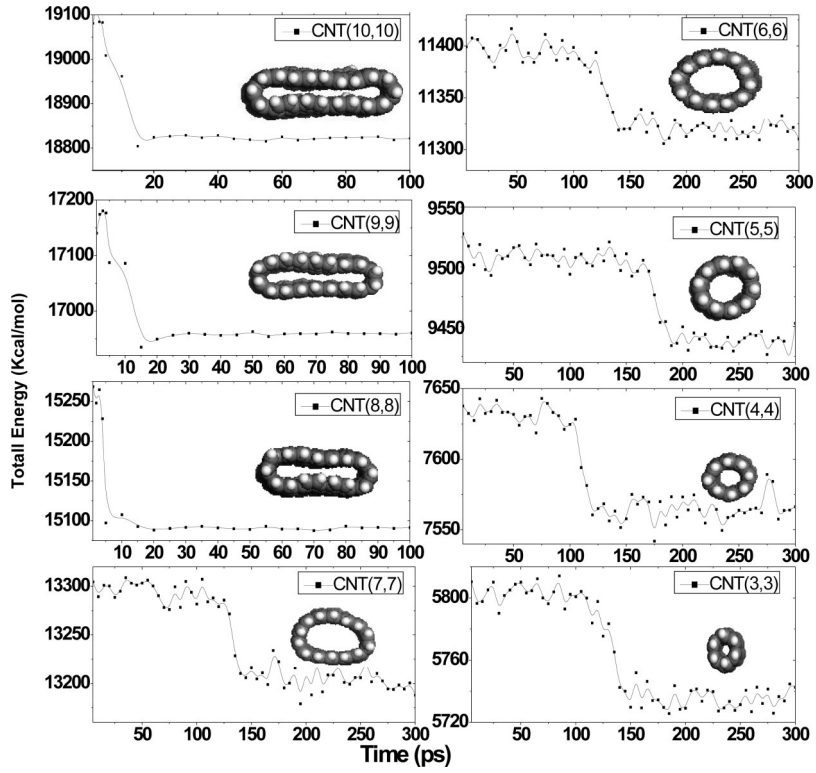

Figure 4. Diameter dependence of armchair CNTs on the total energy of the CNT−Cu_2O system during the simulations.

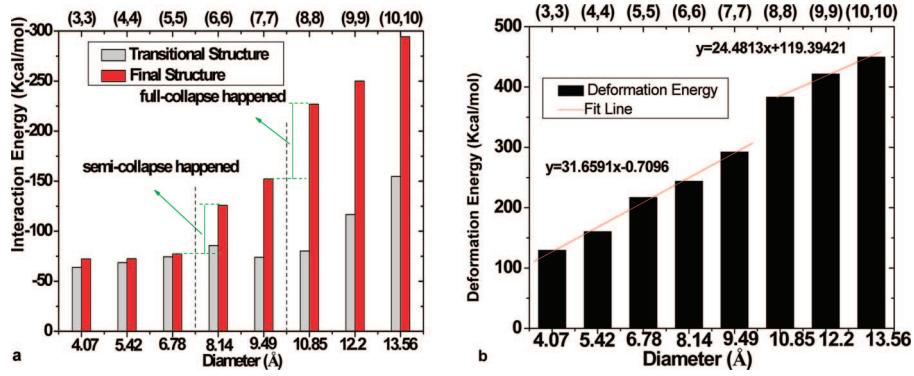

Figure 5. (a) Final interaction energies of the armchair CNT−Cu_2O systems; (b) final deformation energies of the CNTs.

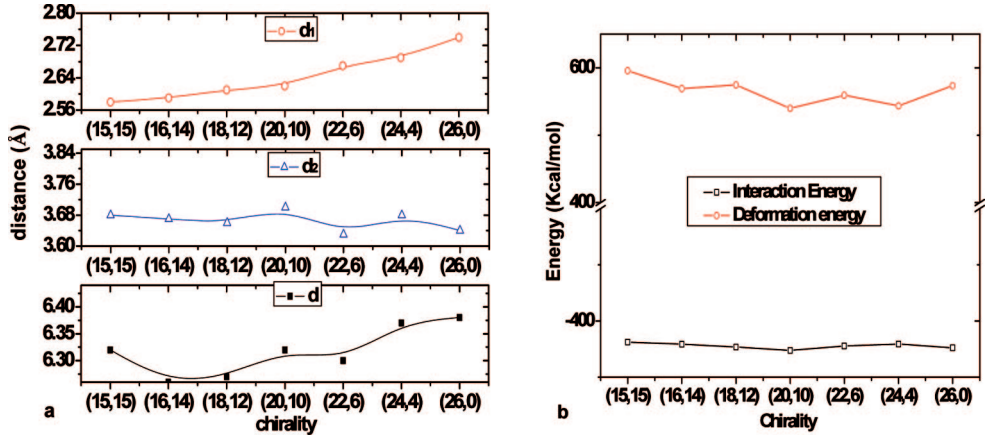

Figure 6. (a) d_1, d_2, and d variations of the collapsed CNTs with chirality; (b) interaction energy and deformation energy variations of the collapsed CNTs with chirality.

properties of CNTs are highly isotropic with little directional dependence.[18]

Moreover, the approach and collapse process is not sensitive to the initial position of the CNTs relative to the Cu_2O surface and the CNT's boundary saturation effect. Moving the initially aligned CNTs away from the Cu_2O surface in the range of the cutoff distance or changing the orientation of the CNTs, the CNTs will finally approach the Cu_2O surface, collapse, and

adhere to the Cu_2O surface by the van der Waals interaction. As the CNTs' length is long enough, the boundary saturation effect is also unconspicuous in our simulations, which indicates that a little tip defects will not determine whether the CNTs collapse or not.

4. Conclusion

We studied the radial collapse of single-walled CNTs on the Cu_2O surface using MD simulations. When the diameter of the CNTs exceeds a threshold the CNTs approach the Cu_2O surface and collapse spontaneously by the van der Waals force between the CNTs and the Cu_2O surface. Because the collapsed CNTs are much more like graphenes, this collapse process of CNTs seems to be the reverse process of folding graphene nanoribbons to form CNTs.

Although the collapse costs large deformation energy and the total energies of the CNTs increase, the total energy of the whole system still behaves as a reduction process due to the approach and collapse of the CNTs. Here, the van der Waals force between them, which is often thought of as a weak force, plays a great role in this approach and serious deformation behaviors. The CNT collapse on the Cu_2O surface is determined by the CNT's diameter size but is not dependent on the chirality, length, placement, and boundary saturation. The collapsed CNTs act as linked graphene ribbons and have the largest area to contact with the Cu_2O surface, which greatly enhances the adhesion between the CNTs and the Cu_2O surface, so the system is much more stable than ever. Due to the hydrophobic properties of the CNTs, the collapsed CNTs on the oxide surface can isolate the metal oxide from water solution, suggesting that the collapsed CNTs on the metal oxide surfaces have potential applications in corrosion protection and scale inhibition fields.

Acknowledgment. This work was supported by the 973 National Basic Research Program (No. 2008CB617508), Cultivation Fund of the Key Scientific and Technical Innovation Project (No. 708061), Ministry of Education of China, and Scientific Research Innovation Foundation of the Graduate School of China University of Petroleum.

References and Notes

(1) Iijima, S. *Nature* **1991**, *354* (6348), 56–58.
(2) Treacy, M. M.; Ebbesen, T. W.; Gibson, J. M. *Nature* **1996**, *381* (6584), 678–680.
(3) Kawano, T.; Chiamori, H. C.; Suter, M.; Zhou, Q.; Sosnowchik, B. D.; Lin, L. *Nano Lett.* **2007**, *7* (12), 3686–3690.
(4) Lourie, O.; Cox, D. M.; Wagner, H. D. *Phys. Rev. Lett.* **1998**, *81* (8), 1638–1641.
(5) Li, J.; Ng, H. T.; Cassell, A.; Fan, W.; Chen, H.; Ye, Q.; Koehne, J.; Han, J.; Meyyappan, M. *Nano Lett.* **2003**, *3* (5), 597–602.
(6) Chopra, N. G.; Benedict, L. X.; Crespi, V. H.; Cohen, M. L.; Louie, S. G.; Zettl, A. *Nature* **1995**, *377* (14), 135–138.
(7) Zang, J.; Treibergs, A.; Han, Y.; Liu, F. *Phys. Rev. Lett.* **2004**, *92* (10), 105501−1–4.
(8) Tangney, P.; Capaz, R. B.; Spataru, C. D.; Cohen, M. L.; Louie, S. G. *Nano Lett.* **2005**, *5* (11), 2268–2273.
(9) Elliott, J. A.; Sandler, J. K. W.; Windle, A. H.; Young, R. J.; Shaffer, M. S. P. *Phys. Rev. Lett.* **2004**, *92* (9), 095501−1–4.
(10) Xiao, J.; Liu, B.; Huang, Y.; Zuo, J.; Hwang, K. C.; Yu, M. F. *Nanotechnology* **2007**, *18* (39), 395703−1–7.
(11) Chopra, N. G.; Ross, F. M.; Zettl, A. *Chem. Phys. Lett.* **1996**, *256* (3), 241–245.
(12) Wu, J.; Zang, J.; Larade, B.; Guo, H.; Gong, X. G.; Liu, F. *Phys Rev. B* **2004**, *69* (15), 153406−1–4.
(13) Maiti, A.; Ricca, A. *Chem. Phys. Lett.* **2004**, *395*, 7–11.
(14) Crespi, V. H.; Chopra, N. G.; Cohen, M. L.; Zettl, A.; Louie, S. G. *Phys. Rev. B* **1996**, *54* (8), 5927–5931.
(15) Xia, Z.; Riester, L.; Curtin, W. A.; Li, H.; Sheldon, B. W.; Liang, J.; Chang, B.; Xu, J. M. *Acta. Mater* **2004**, *52* (4), 931–944.
(16) Sun, D. Y.; Shu, D. J.; Ji, M.; Liu, F.; Wang, M.; Gong, X. G. *Phys. Rev. B* **2004**, *70* (16), 165417−1–5.
(17) Cai, J. Z.; Lu, L.; Kong, W. J.; Zhu, H. W.; Zhang, C.; Wei, B. Q.; Wu, D. H.; Liu, F. *Phys. Rev. Lett.* **2006**, *97* (2), 026402-1–4.
(18) Zanf, J.; Aldas-Palacios, O.; Liu, F. *Commun. Comput. Phys.* **2007**, *2* (3), 451–465.
(19) Liu, B.; Yu, M. F.; Huang, Y. G. *Phys. Rev. B* **2004**, *70* (16), 161402−1–4.
(20) Yu, D. C.; Liu, F. *Nano. Lett.* **2007**, *7* (10), 3046–3050.
(21) Kong, J.; Chapline, M. G.; Dai, H. *Adv. Mater.* **2001**, *13* (18), 1384–1386.
(22) Kong, J.; Franklin, N. R.; Zhou, C.; Chapline, M. G.; Peng, S.; Cho, K.; Dai, H. *Science* **2000**, *287* (5453), 622–625.
(23) Collins, P. G.; Bradley, K.; Ishigami, M.; Zettl, A. *Science* **2000**, *287* (10), 1801–1804.
(24) Planeix, J. M.; Coustel, N.; Coq, B.; Brotons, V.; Kumbhar, P. S.; Dutartre, R.; Geneste, P.; Bernier, P.; Ajayan, P. M. *J. Am. Chem. Soc.* **1994**, *116* (17), 7935–7936.
(25) Zhang, Y.; Dai, H. *Appl. Phys. Lett.* **2000**, *77* (19), 3015–3017.
(26) Javey, A.; Guo, J.; Farmer, D. B.; Wang, Q.; Wang, D.; Gordon, R. G.; Lundstrom, M.; Dai, H. *Nano Lett.* **2004**, *4* (3), 447–450.
(27) Maple, J. R.; Hwang, M. J.; Stockfisch, T. P.; Dinur, U.; Waldman, M.; Ewig, C. S.; et al. *J. Comput. Chem.* **1994**, *15* (2), 162–182.
(28) Sun, H. *J. Comput. Chem.* **1994**, *15* (7), 752–768.
(29) Sun, H. *J. Phys. Chem. B* **1998**, *102* (38), 7338–7364.
(30) Sun, H.; Ren, P.; Fried, J. R. *Comput. Theor. Polym. Sci.* **1998**, *8* (1/2), 229–246.
(31) Rigby, D.; Sun, H.; Eichinger, B. E. *Polym. Int.* **1998**, *44* (3), 311–330.
(32) Kisin, S.; Bozovic Vukic, J.; van der Varst, P. G. T.; de With, G.; Koning, C. E. *Chem. Mater.* **2007**, *19* (4), 903–907.
(33) DeRuntz, J. A.; Hodge, P. G. *J. Appl. Mech.* **1963**, *30*, 391–395.
(34) Gupta, N. K.; Sekhon, G. S.; Gupta, P. K. *Thin Wall. Struct.* **2005**, *43* (6), 895–922.
(35) Chang, T. C. *Phys. Rev. Lett.* **2008**, *101* (17), 175501-1–4.

JP808264D